

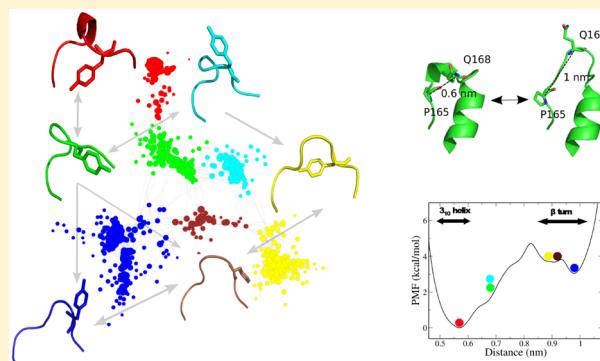
Evolutionary Conserved Tyr169 Stabilizes the $\beta 2$ - $\alpha 2$ Loop of the Prion Protein

Danzhi Huang* and Amedeo Caflisch*

[†]Department of Biochemistry University of Zürich, Winterthurerstrasse 190, CH-8057 Zürich, Switzerland

S Supporting Information

ABSTRACT: Experimental evidence indicates that the primary structure of the $\beta 2$ - $\alpha 2$ loop region (residues 165–175) in mammalian prion proteins (PrP) influences the conversion from the cellular species (PrP^C) to the β -sheet-rich aggregate. Here, we captured the transition of the $\beta 2$ - $\alpha 2$ loop from 3_{10} -helical turn to β turn by unbiased molecular dynamics simulations of the single-point mutant Y169G. Multiple conformations along the spontaneous transition of the mutant were then used as starting point for sampling of the free-energy surface of the wild type and other single-point mutants. Using two different methods for the determination of free energy profiles, we found that the barrier for the 3_{10} -helical turn to β turn transition of the wild type is higher by about 2.5 kcal/mol than for the Y169G mutant, which is due to favorable stacking of the aromatic rings of Y169 and F175, and a stable hydrogen bond between the side chains of Y169 and D178. The transition of the $\beta 2$ - $\alpha 2$ loop to β turn increases the solvent-exposure of the hydrophobic stretch 169-YSNQNNF-175. The simulations indicate that the strictly conserved Y169 in mammalian prion proteins stabilizes the 3_{10} -helical turn in the $\beta 2$ - $\alpha 2$ loop, thus hindering the conversion to an aggregation-prone conformation.



1. INTRODUCTION

The function of the prion protein (PrP) in mammals is not known. Experimental evidence has accumulated indicating that prion diseases, which can lead to epidemics as in the case of bovine spongiform encephalopathy,¹ are associated with PrP aggregates. These aggregates can autocatalyze the conversion and aggregation of the cellular PrP (PrP^C),² but the mechanism of conversion is also not clear.

Nuclear magnetic resonance (NMR) spectroscopy has demonstrated that the PrP^C in mammals has a disordered N-terminal segment of about 100 residues and a folded C-terminal domain (about 110 residues) consisting of three α -helices and a two-stranded antiparallel β -sheet.³ Detailed NMR line shape analyses have been reported for the $\beta 2$ - $\alpha 2$ loop, which consists of residues 165–175 and links the second β -strand to the second α helix. The NMR studies show that the $\beta 2$ - $\alpha 2$ loop in the mouse prion protein forms a 3_{10} -helical turn (at residues 165–168) at 37 °C, shows local conformational polymorphism at 20 °C, and forms a β turn (at residues 167–170) for the mutants Y169G and Y169A.^{3–6} It is important to note that Y169 is strictly conserved in mammalian PrPs. In addition, mouse and human prion proteins share the 169-YSNQNNF-175 heptapeptide segment. This 7-residue segment has high sequence similarity to the fibril-forming GNNQQNY heptapeptide from the yeast prion protein Sup35.⁷ Moreover, the SNQNNF hexapeptide has been shown to form steric zipper amyloid-like fibrils.⁸

Recently, Sigurdson and collaborators have investigated the influence of modifications of the $\beta 2$ - $\alpha 2$ loop on prion transmission *in vivo*⁹ and prion conversion *in vitro*.¹⁰ Interestingly, transgenic mice expressing the triple-point mutant Y169G, S170N, and N174T (where the two latter substitutions were previously reported to stabilize a “rigid loop”⁴) could not be infected by mouse prions (two strains) or deer chronic wasting disease prions.⁹ These *in vivo* results suggest that Y169 plays an important role in prion formation, and taken together with the NMR spectroscopy data⁵ they provide evidence that structural changes in the $\beta 2$ - $\alpha 2$ loop modulate prion aggregation. The *in vitro* prion conversion assay was used to analyze the effect of mutations on the conversion of PrP^C to the aggregation-prone conformation,¹⁰ and the assay results were interpreted according to the “steric zipper” model obtained by X-ray diffraction of SNQNNF microcrystals.⁸ The *in vitro* data suggest that an aromatic residue at position 169 promotes prion conversion because of optimal packing of pairs of in-register parallel β -sheets in the steric zipper.¹⁰ Collectively, the NMR spectroscopy studies, prion conversion assay data, and *in vivo* evidence suggest that the side chain of the strictly conserved Y169 plays a physiological role.

The mouse PrP^C has been investigated by several molecular dynamics (MD) simulation studies^{11,12,14} since its structure in

Received: November 11, 2014

Published: February 11, 2015

Table 1. Simulations Performed

protein	sequence	pH ^a	β 2- α 2 loop conformation	no. of runs	run length (μ s)	β 2- α 2 loop transition
Unbiased Sampling						
Y169G	125–226	neutral	4H88	2	1	yes ^b
Y169G	125–226	neutral	4H88	14	0.03–0.2	yes ^c
Y169A	125–226	neutral	4H88	2	1	no
WT	125–226	neutral	4H88	4	1	no
WT	119–231	neutral	2L39	2	1	no
WT	125–226	low	4H88	4	1	no
WT	121–226	low	4H88	2	1	no
WT	125–226	neutral	β turn 1	2	1	no
WT	125–226	neutral	β turn 2	2	1	no
WT	125–226	neutral	intermediate	200	0.01 or 0.04	yes
WT	125–226	neutral	along transition pathway	100	0.01	yes
Umbrella Sampling						
WT	125–226	neutral	along transition pathway	23	0.05	no ^d
mutants ^e	125–226	neutral	along transition pathway	23	0.05	no ^d

^aWild type (WT) simulations were carried out with the side chain of the three histidines protonated on a single nitrogen atom (six runs) or both nitrogen atoms (i.e., positively charged, six runs) to emulate neutral or low pH conditions, respectively. ^bOne and two transitions in the first and second run, respectively. ^cTransitions were observed in 8 of 14 runs. ^dTransitions are not possible as the umbrella potential restricts the motion along the coordinate that describes the transition itself, i.e., the distance between C α atoms of residues 165 and 168. ^eThe mutants are Y169G, Y169A, Y169F, R164A, F175A, and D178A.

solution was solved by NMR spectroscopy.³ These simulation studies focused on the mouse and the mouse/elk hybrid prion proteins,¹¹ pathological mutants of the human prion protein,¹² and mutants linked to scrapie resistance.¹⁴ Evidence has been provided for the structural plasticity of the β 2- α 2 loop,^{11,13} but the role of residue Y169 has not been elucidated.

Here, we use MD to investigate the plasticity of the β 2- α 2 loop and to shed light on the role of Y169. First, MD simulations of the Y169G mutant of the mouse prion protein were carried out to enhance the transition between the 3₁₀-helical turn (involving residues 165-PVDQ-168) and β turn conformation (residues 167-DQYS-170) of the β 2- α 2 loop. These simulations were started because of the lack of transitions during multiple 1- μ s MD simulations of the wild type, and were inspired by NMR spectroscopy data that suggested a very large population of the β turn conformation for the Y169G mutant.⁵ Multiple MD snapshots saved along the spontaneous transitions of the Y169G mutant were used to start unbiased MD simulations of the wild type and perform umbrella sampling potential of mean force (PMF) calculations and cut-based free energy profile analysis^{15,16} of wild type and several single-point mutants. The MD simulation results indicate that the wild type Y169 has a higher free energy barrier for the conversion to the β turn conformation than the Y169G, Y169A, Y169F, R164A, F175A, and D178A single-point mutants.

2. RESULTS AND DISCUSSION

We first describe the spontaneous transition of the β 2- α 2 loop from 3₁₀-helical turn to β turn which took place in unbiased MD runs of the Y169G mutant but not in those of Y169A or wild type on a 1- μ s time scale (Table 1). We then compare the conformational space of wild type and Y169G mutant by network analysis. Next, we determine the free energy profile of the β 2- α 2 loop transition using umbrella sampling and two different methods for projecting the free energy. In the Conclusions section, we list the biological implications of the combined analysis of simulation results and experimental data,

and propose simulations of a glycine mutant as a general strategy for enhancing the sampling of rare events.

2.1. Spontaneous Transition of the β 2- α 2 loop in Unbiased Simulations of the Y169G Mutant. We hypothesized that the Y169G mutation would facilitate the rearrangement of the β 2- α 2 loop because of the loss of favorable interactions between the Y169 side chain and residues F175 and D178 (Figure 1, top right), as well as the reduced steric hindrance of glycine. Three spontaneous transitions of the β 2- α 2 loop from the 3₁₀-helical turn (involving residues 165-PVDQ-168) to a β turn (residues 167-DQYS-170) were observed in two 1- μ s runs of the Y169G mutant (Figure 1, bottom, and Supporting Information Figure SI3). Note that the 3₁₀-helical turn and the β turn are mutually exclusive because of their (partial) overlap in primary structure. The β turn is stabilized by a 170NH-CO167 or 169NH-CO166 backbone hydrogen bond (Supporting Information Figure SI1). In addition, the hydroxyl group of S170 acts as donor to the carbonyl oxygen and acceptor from the amide nitrogen of residue 167 in about 15% and 6%, respectively, of the snapshots (Supporting Information Figure SI1).

In contrast to the simulations of Y169G, the 3₁₀-helical turn was stable in two 1- μ s runs of the Y169A mutant and 12 1- μ s runs of the wild type (10 started from the X-ray structure, PDB 4H88, and 2 started from NMR structure, PDB 2L39) with different initial velocities (Supporting Information Figures SI2 and SI3). The structural stability of the 3₁₀-helical turn does not seem to depend on the pH as the wild type simulations did not show any transition at neutral or low pH conditions (see Table 1 and Supporting Information Figure SI2). These simulation results suggest that the free energy barrier for the unfolding of the 3₁₀-helical turn is much higher for the wild type than the Y169G mutant which was further verified by PMF umbrella sampling calculations and cut-based free energy profile analysis^{15,16} (see below).

2.2. Side Chain of Y169 Stabilizes the 3₁₀-Helical Turn Conformation. It is useful to project the conformational space of a system with many degrees of freedom into a two-dimensional representation that qualitatively illustrates the

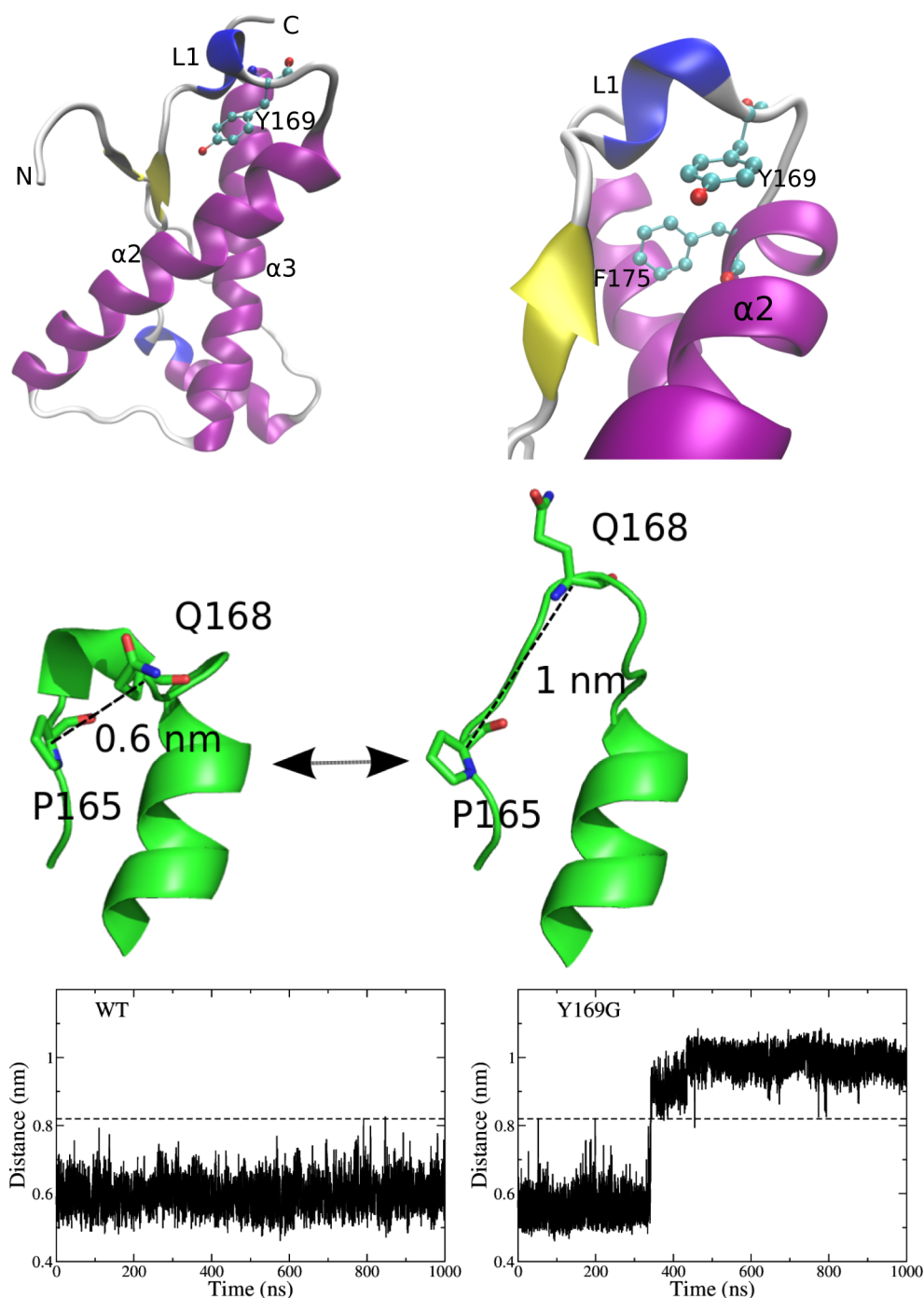


Figure 1. Conformational transition of the $\beta 2$ - $\alpha 2$ loop (residues 165–175) is observed only in simulations of the Y169G mutant within a 1- μ s time scale. (Top) Structure of the prion protein with labels for secondary structure elements. The $\beta 2$ - $\alpha 2$ loop is labeled L1. (Middle) The distance between the C_{α} atoms of residues P165 and Q168 (dashed line) is used to monitor the transition of the $\beta 2$ - $\alpha 2$ loop from 3_{10} -helical turn (left) to β turn (right). Note that the 3_{10} -helical turn is formed by residues 165-PVDQ-168 while the β turn involves residues 167-DQYS-170. (Bottom) Time series of the distance between the C_{α} atoms of P165 and Q168 in a simulation of the wild type (left) and Y169G mutant (right). A transition is observed for the Y169G mutant but not for the wild type.

transitions between mesostates. The network analysis of MD simulations provides a qualitative description of the main mesostates (i.e., clusters of snapshots) and transitions between them as sampled along the MD trajectories.¹⁷ The network analysis of the unbiased Y169G simulations reveals that the $\beta 2$ - $\alpha 2$ loop directly transits from the 3_{10} -helical turn to the β turn (Figure 2, top left). The β turn conformation consists of two substates (clusters of green and blue nodes in Figure 2 top and

Supporting Information Figure SI7). Interestingly, the loop conformations in the substates of green nodes are similar to the NMR structure of mouse Y169G mutant (PDB 2L1D, Supporting Information Figure SI4); i.e., they have a root-mean-square deviation (RMSD) smaller than 2 Å for the C_{α} atoms of residues 166–170 upon structural overlap of the C_{α} atoms in helices $\alpha 2$ and $\alpha 3$, while for the blue nodes the corresponding RMSD is more than 4 Å.

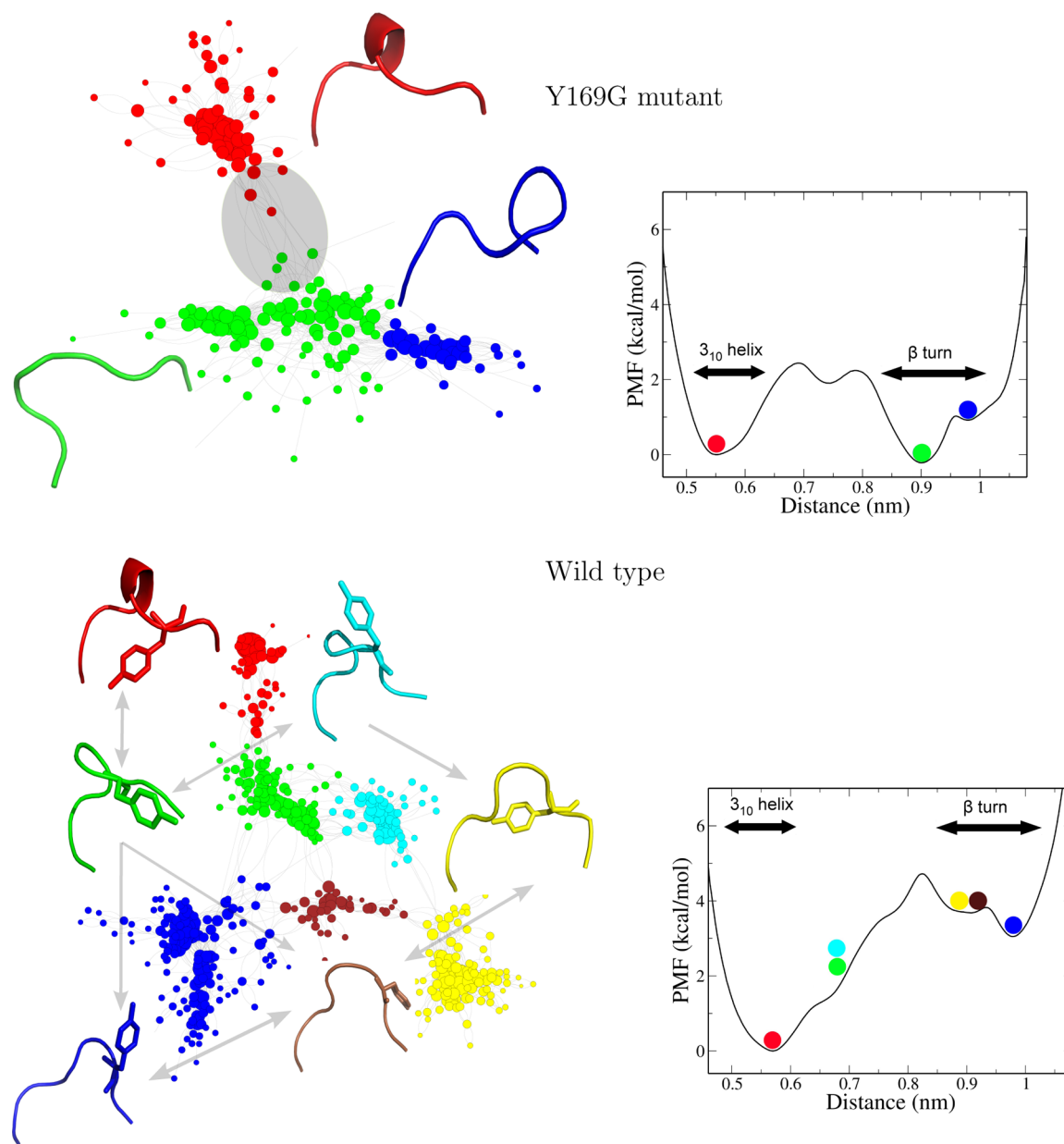


Figure 2. Pathways and free energy profile of Y169G mutant (top) and wild type (bottom) mouse PrP^C. (Left) Complex network analysis¹⁷ of the $\beta 2$ - $\alpha 2$ loop conformational space and transitions observed in the MD simulations. Nodes are clusters of MD snapshots, and links are transitions between them as observed in the MD trajectories. Metastable states are colored individually, and a representative conformation is shown for each metastable state. Nodes used for enhanced sampling of the $\beta 2$ - $\alpha 2$ loop transition of the wild type are emphasized (gray ellipse). (Right) Profiles of the PMF along the distance between the C α atoms of P165 and Q168, which reflects the $\beta 2$ - $\alpha 2$ loop transition. The colored circles correspond to the metastable states and structural representatives shown in the network.

For the wild type, two metastable states (clusters of green and cyan nodes in Figure 2, bottom) are identified along the transition. In these states, the hydrogen bond between the side chains of Y169 and D178 is broken and Y169 is displaced from its initially buried orientation while the 3_{10} -helical turn is still present. Finally, the helical conformation opens up followed by formation of the β turn, which consists of multiple substates (clusters of blue, brown, and yellow nodes in the bottom of Figure 2).

The network analysis suggests multiple states with free-energy barriers between them. To obtain a quantitative description of the free-energy surface of the transition, PMF profiles were extracted from umbrella sampling along a progress variable that distinguishes between presence and absence of the

3_{10} -helical turn. The free-energy barrier on the PMF profile for the conversion from 3_{10} -helical turn to β turn is higher by about 2.5 kcal/mol for the wild type than the Y169G mutant (Figure 3). Moreover, the 3_{10} -helical turn is thermodynamically more stable than the β turn in the wild type but not in the Y169G mutant. The distance between C α atoms of residues P165 and Q168 is a simple and intuitive geometric variable which can be used to qualitatively describe the kinetics of the transition. Along this progress variable, the position corresponding to the free-energy maximum shifts toward the destabilized (i.e., 3_{10} -helical) state for the Y169G mutant, which is consistent with Hammond behavior.¹⁸ It is important to note that a quantitative description of the shift of the transition state is

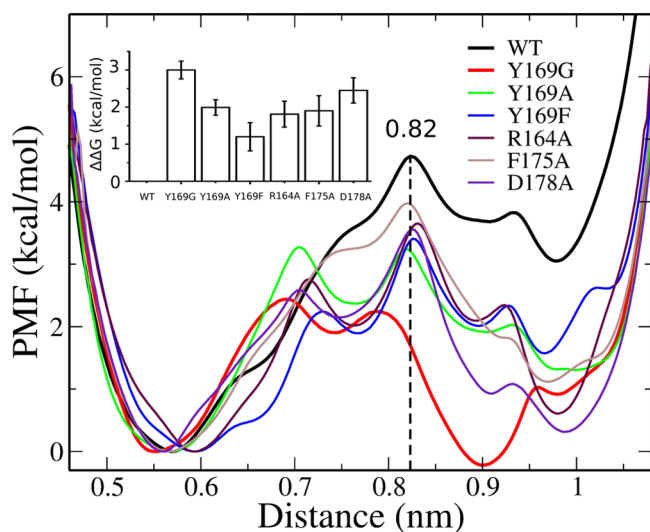


Figure 3. Profiles of the PMF along the distance between the C_{α} atoms of P165 and Q168 which reflects the $\beta 2$ - $\alpha 2$ loop transition. Evidence for statistical convergence of the umbrella sampling is shown in the Supporting Information (Figure SI9). (Inset) Influence of mutations on the thermodynamic stability of the 3_{10} -helical turn conformation. The free energy difference between 3_{10} -helical turn and β turn states was calculated by integrating the PMF for values of the distance between the C_{α} atoms of P165 and Q168 < 0.82 nm and ≥ 0.82 nm, respectively. The free energy difference for the wild type is set to zero (reference value). The error bars were determined by block averaging, i.e., by calculating each PMF twice, once over the 10–30 ns simulation interval and once over the 30–50 ns interval.

not possible because it would require the knowledge of the reaction coordinate.

Additional PMFs were calculated with the same protocol as for wild type and the Y169G mutant to evaluate the contribution of individual side chains to the stabilization of the 3_{10} -helical turn (Figure 3). The free energy barrier for the transition is lower in all simulated mutants (Y169G, Y169A, Y169F, R164A, F175A, and D178A) than in the wild type, indicating that interactions between Y169 and the F175 and D178 side chains stabilize the 3_{10} -helical turn and slow down the conformational transition of loop $\beta 2$ - $\alpha 2$. These interactions are further supported by the SAPHIRE (states and pathways projected with high resolution) analysis which provides a comprehensive picture of the thermodynamics and kinetics of complex systems.^{19,20} The SAPHIRE plot of the wild type mouse PrP^C shows that the 3_{10} -helical turn is stabilized by the close packing of Y169 and F175 as well as a hydrogen bond between the side chains of Y169 and D178 (Figure 4). Moreover, favorable polar interactions (direct salt bridge or water-bridged ionic interaction) between R164 and D178 (Supporting Information Figure SI10) orient the side chain of D178 toward the hydroxyl of Y169. Thus, the wild type has the most stable 3_{10} -helical turn (which is consistent with the lack of transitions along the unbiased simulations) followed by the Y169F mutant, whereas the Y169G and D178A mutants show the worst stability of the 3_{10} -helical turn. Quantitatively, integration of the PMF along the distance between C_{α} atoms of residues P165 and Q168 individually for wild type and each mutant yields a destabilization of the 3_{10} -helical turn (relative to wild type) of 3.0 kcal/mol for Y169G, 2.5 kcal/mol for D178A, 2.0 kcal/mol for Y169A, 1.9 kcal/mol for F175A, 1.8 kcal/mol for R164A, and 1.2 kcal/mol for Y169F (inset of Figure 3).

These simulation results are in agreement with the NMR spectroscopy data which show that an aromatic side chain at position 169 is required to maintain the 3_{10} -helical turn conformation of the loop $\beta 2$ - $\alpha 2$.⁵ Moreover, the PMF profile of the F175A mutant (brown curve in Figure 3) is consistent with the NMR solution structure of the single-point mutant F175A which shows a well-defined 3_{10} -helical turn.²¹

2.3. Kinetic Analysis of the Trajectories. The PMF profile is a histogram-based projection of a complex multi-dimensional free energy surface onto an *a priori* chosen progress variable. In contrast, the cut-based free energy profile, which is calculated from the transition matrix, takes into account all of the kinetic information, i.e., all pathways to the reference state.^{15,16} The PMF profile has the advantage of the simple and physically intuitive geometric distance used as progress variable, whereas in the cut-based free energy profile the reaction coordinate is more difficult to interpret. Importantly, the PMF profiles (Figure 3) and cut-based free energy profiles (Figure 5) provide a consistent picture. In particular, the highest free energy barrier is observed for the wild type in both profiles, followed by the D178A, Y169F, and Y169G mutants. These differences in the free energy barrier provide an explanation for recent *in vitro* experiments, which have shown that the prion aggregation conversion of Y169F is about 20% higher compared to wild type over a 24-h period.¹⁰ On the other hand, the transition from 3_{10} -helix to β turn in the mutant Y169G is faster than wild type according to the simulations whereas the *in vitro* experiments show reduced aggregation.¹⁰ Taken together, the simulation and *in vitro* data for Y169G suggest that the lack of the aromatic side chain (important for ordered aggregation^{22,23}) overrides the faster transition and higher stability of the β turn conformation of the $\beta 2$ - $\alpha 2$ loop.

2.4. Solvent Exposure of the Y169 Side Chain. A plethora of computational and experimental data provides strong evidence that amyloid-like aggregation can be promoted by inter(poly)peptide interactions involving aromatic side chains. This evidence ranges from atomistic simulations of short peptides²² to *in vitro* prion conversion assays¹⁰ and *in vivo* experiments with transgenic mice.⁹ Here, we analyze the solvent accessibility of the Y169 residue as solvent exposure of the aromatic side chain in the monomeric state is expected to facilitate aggregation.

The complex network analysis (Figure 2) and SAPHIRE plot (Figure 4) suggest that rupture of the 3_{10} -helical turn results in conformational variability, particularly for the wild type. The PMF is plotted in Figure 6 along the distance between the Y169 side chain and the $\alpha 3$ helix (C_{α} atom of E221, see Methods section). This PMF indicates that there are multiple orientations of the Y169 side chain in the β turn conformation of the $\beta 2$ - $\alpha 2$ loop. The yellow node labels a region of the PMF profile in which the phenol ring of Y169 interacts with the $\alpha 3$ helix by favorable contacts with the side chains of V166, F175, Y218, E221, and Y225. It is interesting to note that Y218 is strictly conserved in mammalian prion proteins, and V166, F175, and E221 are conserved.^{24,25}

The blue node consists of conformations with the Y169 side chain pointing to the solvent. Thus, the polymorphism of the $\beta 2$ - $\alpha 2$ loop is due not only to the backbone, i.e., transitions between the 3_{10} -helical turn and β turn, but also to variable orientations of the Y169 side chain within the β turn state. The distribution of the solvent accessible surface (SAS) of the 169-YSNQNNF-175 segment along the MD simulations of the wild

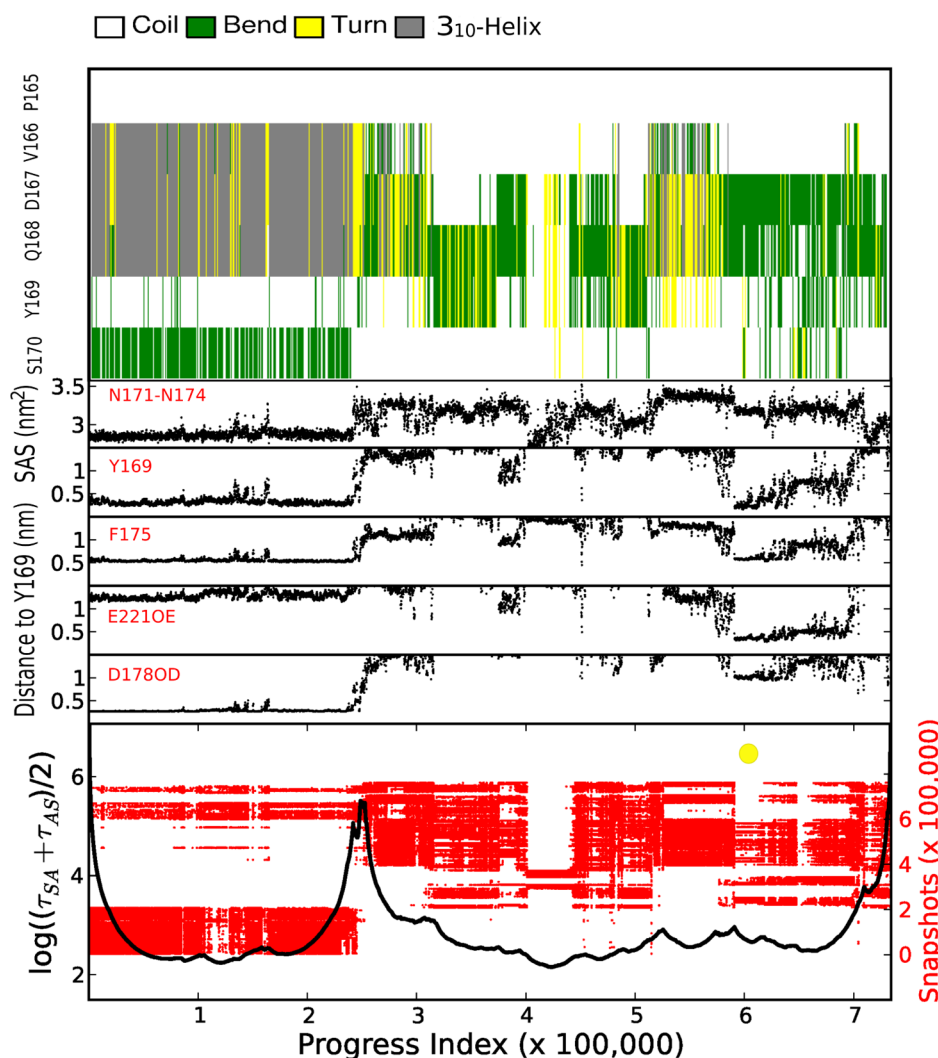


Figure 4. Structural analysis of the 3_{10} -helical state and the β turn state of the $\beta 2$ - $\alpha 2$ loop. SAPHIRE plot¹⁹ for wild type mouse PrP^C. The 730 000 snapshots saved along nearly 15 μ s of MD trajectories are ordered according to the structure of the $\beta 2$ - $\alpha 2$ loop. The resulting order is called progress index and is annotated with kinetic information (black profile in panel on bottom, legend on left y -axis) and dynamical trace (red dots, legend on right y -axis).²⁰ The kinetic information reflects the mean first passage time $(\tau_{SA} + \tau_{AS})/2$ of a two-state Markov state model.¹⁹ The remaining panels (from bottom to top) show the distance of the Y169 hydroxyl oxygen to the closest carboxyl oxygen of D178 or E221, the distance of the mass center of the phenol ring of Y169 to the side chain of F175, the solvent accessible surface (SAS) of the side chain of residues 169 or 171-NQNN-174, and the DSSP assignment⁴² by residue (legend on top). It is important to note that the progress index sorts all snapshots and does not require clustering. On the other hand, to improve visibility the distance and SAS values are shown as averages over 100 snapshots, while the DSSP assignment is shown for every 1000th snapshots along the progress index. The barrier at a progress index value of about 250 000 separates the 3_{10} -helical from the β turn state. The yellow circle in the bottom panel emphasizes the β turn substate with buried Y169 which corresponds to the first minimum in the PMF profile in the right panel of Figure 6.

type shows that it is more exposed in the β turn than in the 3_{10} -helical turn conformation of loop $\beta 2$ - $\alpha 2$ (Figure 7). The increase of nearly 1.5 nm² (from the 3_{10} -helical peak at about 4.6 nm² to the β turn peak at about 6.0 nm²) is due mainly to the increase in exposure of the Y169 side chain and only slightly to N171 and N174 (Supporting Information Figure SI11). This finding is corroborated by the essentially identical solvent exposure of the 169-GSNQNNF-175 segment in the 3_{10} -helical turn and β turn conformations of the Y169G mutant (Supporting Information Figure SI8). The remaining single-point mutants show a higher solvent exposure of the 169–175 segment in going from 3_{10} -helical turn to β turn, and the increase is similar to the wild type (for Y169F) or smaller (Supporting Information Figures SI5 and SI6).

A combined experimental (X-ray crystallography and NMR spectroscopy) and simulation study has recently shown that the antiprion activity of tricyclic phenothiazine compounds originates from the allosteric stabilization of several motifs of the PrP^C structure, including the $\beta 2$ - $\alpha 2$ loop.²⁶ Interestingly, the specific binding of promazine (to a pocket located close to the $\alpha 2$ helix) stabilizes the 3_{10} -helical turn of the $\beta 2$ - $\alpha 2$ loop by the allosteric formation of a hydrogen bond network involving the Y169 and D178 side chains (PDB 4MA7). These structural data, taken together with the antiprion property of promazine, provide evidence that the solvent exposed conformation of Y169 is linked to aggregation. Concerning the residues that stabilize Y169 in a buried orientation, our simulation results and the X-ray crystallography data²⁶ suggest that mutations at D178 (e.g., the single point mutants D178A or D178N) and/or

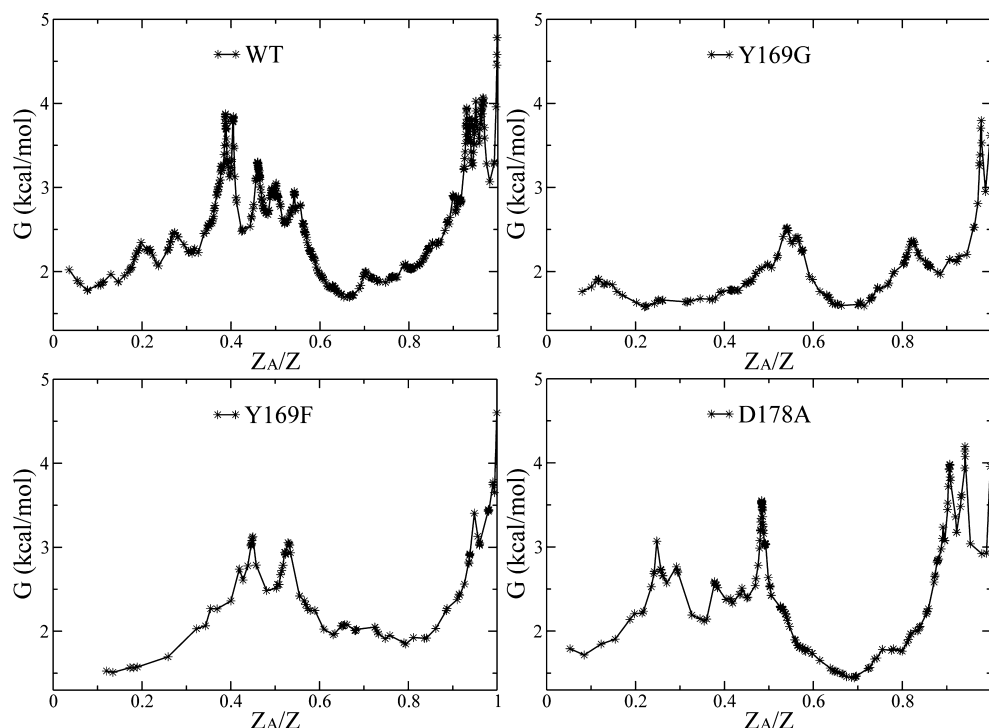


Figure 5. Cut-based free energy profile for wild type mouse PrP^C, and the single-point mutants Y169G, Y169F, and D178A. The most populated node in the 3_{10} -helical turn is used as reference and is the first data point on the left of each panel. The relative partition function Z_A/Z is a reaction coordinate that takes into account all pathways to the reference state.¹⁵ Note that both the PMF profiles (Figure 3) and the cut-based free energy profiles are projections on a single dimension. The PMF profile is an histogram-based projection on the geometric distance used in the umbrella sampling protocol whereas the cut-based free energy profile does not require any *a priori* selection of reaction coordinate.

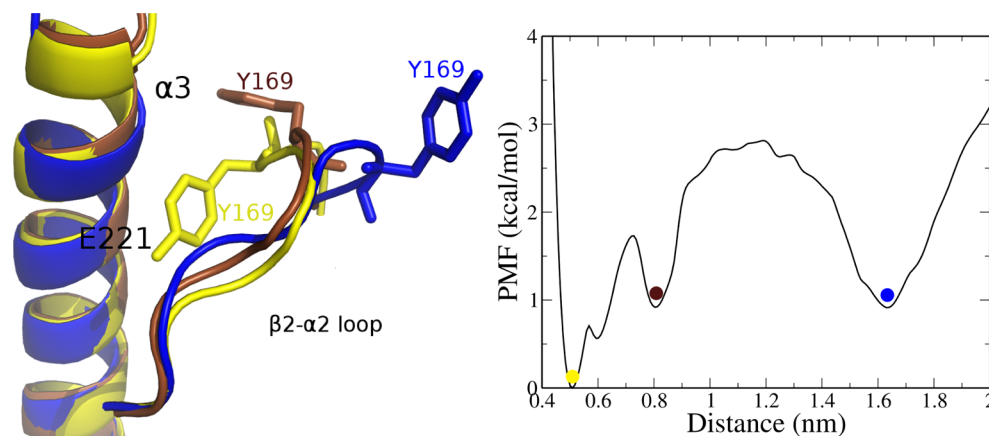


Figure 6. Multiple substates within the β turn state. (Left) Three MD snapshots with different degree of Y169 burial within the β turn state. (Right) The PMF is plotted along the distance between the C_α atom of residue E221 in helix 3 and the center of the phenyl ring of Y169. The positions of the three snapshots are emphasized by circles in the PMF, and the colors are consistent with those in the left panel and in Figure 2, bottom, right panel. Note that the free energy barrier (of about 3 kcal/mol) is visible in this PMF and not in the bottom, right panel of Figure 2 because the progress variable used for this PMF is more appropriate than the one in the PMF of Figure 2 in which the projection almost completely suppresses the barrier.

R164 should facilitate prion aggregation, which could be verified by the *in vitro* prion conversion assay¹⁰ followed by experiments on transgenic mice. In this context, it is important to note that the familial (i.e., hereditary) form of fatal insomnia and Creutzfeldt-Jakob disease are linked to the D178N mutation.²⁷

2.5. Conclusions. We have carried out MD simulations to investigate the local conformational polymorphism of the $\beta 2$ - $\alpha 2$ loop in the wild type prion protein and six single-point mutants, three of the strictly conserved Y169 and three of residues that

interact with it. The PMF profiles (Figure 3) and cut-based free energy profiles (Figure 5) provide a quantitative description of the relative stability of 3_{10} -helical turn and β turn conformations as well as the free-energy barrier separating them. The following conclusions can be drawn from the combined analysis of the MD simulations and experimental results: (1) The 169-YSNQNNF-175 segment is more exposed to solvent in the β turn than the 3_{10} -helical turn conformation of the loop $\beta 2$ - $\alpha 2$ (Figure 7). It is important to note that higher solvent exposure of Y169 has been linked to cytotoxicity.^{26,28}

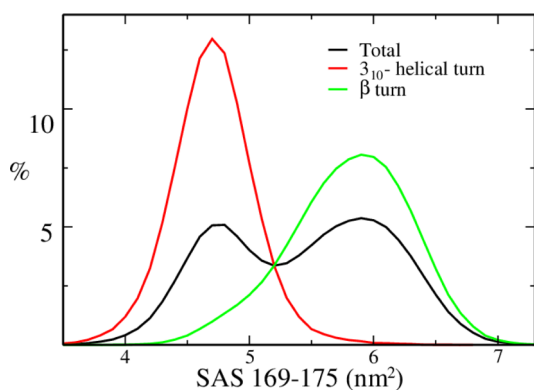


Figure 7. Distribution of solvent accessible surface (SAS) of residues 169–175 for the nearly 15 μ s of unbiased sampling of the wild type. Individual snapshots were assigned to the 3_{10} -helical state or β turn state according to the SAPPHERE plot (Figure 4).

Interestingly, this 7-residue segment has a high sequence similarity to the fibril-forming GNNQQNY heptapeptide from the yeast prion protein Sup35.⁷ Furthermore, the SNQNNF hexapeptide has been shown to form steric zipper amyloid-like fibrils.⁸ (2) The strictly conserved Y169 in the middle of the β 2- α 2 loop (residues 165-PMDEYSNQN-175 in human and 165-PVDQYSNQN-175 in mouse) is required to stabilize the 3_{10} -helical turn and thus hinder the transition to the β turn (Figures 3 and 5). (3) The conserved residues F175 and D178 interact directly with Y169 in the 3_{10} -helical turn conformation of the β 2- α 2 loop (Figure 4) and disfavor the transition to the β turn (Figure 3). Moreover, the basic residue at position 164 (R or K in mammalian prion proteins) is involved in a direct or water-bridged ionic interaction with the side chain of D178. The ionic interaction stabilizes the D178 side chain in an orientation that favors its hydrogen bond with the hydroxyl group of Y169. (4) The β turn conformation is heterogeneous and consists of several metastable states (Figure 6). The Y169 side chain has variable solvent exposure, which is modulated by interactions with the following side chains: V166, F175, Y218, E221, and Y225. Except for Y225, the residues interacting with Y169 in the β turn conformation are highly conserved in mammalian prion proteins. (5) For the Y169G mutant, the shift of the transition state toward the destabilized 3_{10} -helical turn state (Figure 3) is an example of Hammond behavior.

Finally, we propose the simulation of a glycine mutant as a strategy for sampling initial pathways of conformational transitions that are too slow to be accessible by MD simulations of the wild type protein. The initial pathway(s) can be used for starting multiple independent simulations of the wild type protein and/or other mutants as in this work. This strategy should be useful in general for the simulation-based free energy analysis of conformational transitions in protein loops.

METHODS

Simulation Protocols. The coordinates of wild type mouse PrP^C were downloaded from the protein database (PDBs 4H88 and 2L39).²⁹ The side chains of aspartates and glutamates were negatively charged, those of lysines and arginines were positively charged, and for simulations at pH 7.0 or 4.5, all histidine side chains (His140, His177, and His187) were neutral or positively charged, respectively. Subsequently, the structure was solvated in a water box whose size was chosen to have a minimal distance of 1.0 nm between the boundary and any atom of the protein. The simulation system

contained sodium and chloride ions to approximate an ionic strength of about 150 mM and to compensate for the total charge of prion. The MD simulations were carried out with Gromacs 4.5.5³⁰ using the CHARMM PARAM36 force field³¹ with virtual site hydrogens³² and the TIP3P model of water.³³

Periodic boundary conditions were applied, and electrostatic interactions were evaluated using the particle-mesh Ewald summation method.³⁴ The van der Waals interactions were truncated at a cutoff of 1.0 nm. The MD simulations were performed at constant temperature (310 K) using the velocity rescaling thermostat and constant pressure (1 atm).³⁵ The LINCS algorithm was used to fix the covalent bonds involving hydrogen atoms and a time step of 5 fs was used in all runs.

Analysis. The analysis of the MD trajectories was carried out with Gromacs 4.5.5³⁰ and the MD-analysis tool WORDOM.³⁶ Clustering according to pairwise RMSD was carried out using the tree like algorithm³⁷ as implemented in CAMPARI.³⁸ First the structural overlap was determined using the C_{α} atoms of the helix α 2 and α 3 residues. Upon overlap of the prion structures the RMSD was evaluated for the C_{α} atoms of the residues 166–170. A threshold of 0.2 nm for the RMSD from the cluster representative was used for assigning a snapshot to a cluster.

The SAPPHERE plots were produced using CAMPARI.³⁸ Starting from an arbitrary snapshot, all the snapshots are sequentially ordered in a stepwise fashion. In each step, the snapshot geometrically closest to any snapshot prior in the sequence becomes the next entry. The aforementioned RMSD was used as geometric distance. The complete sequence of snapshots is called progress index. Assuming high snapshot density within free-energy basins, snapshots belonging to the same basin are grouped together, and distinct states do not overlap.¹⁹

Generation of β 2- α 2 Loop Exchange Pathway. The following 6-step strategy was used to explore the β turn conformations of β 2- α 2 loop and promote the conformational exchange. Step 1 is simulations of the mutant Y169G. The coordinates of Y169G were generated from the mouse prion protein structure (PDB 4H88) by deleting the Y169 side chain. There were 18 MD simulations performed, and the simulation times ranged from 0.03 to 1 μ s. Step 2 is clustering and network analysis of the simulated results. For step 3, the analysis from step 2 revealed two main conformations of β 2- α 2 in β turn. The conformation representatives were identified, and the G169 was mutated back to tyrosine by adding the side chain atoms. The starting conformations were relaxed and equilibrated for 1 ns. Two independent 1- μ s all-atom MD simulations were performed starting from these two conformation representatives, respectively. In step 4, 200 cluster representatives were randomly selected from the clusters in the gray area of Figure 2). The G169 was mutated back to tyrosine, and simulations were performed for 0.010 or 0.04 μ s. For step 5, in the Y169G simulations the transition of β 2- α 2 loop from 3_{10} -helix to β turn was sampled 10 times in 10 independent simulations. For each of these transitions, 10 snapshots were extracted with 0.1 ns interval along the transition pathway. The G169 of all the 100 snapshots was mutated back into tyrosine, and 0.010 μ s simulations were started for each of them. For step 6, the final clustering and network analysis were performed for all simulations of wild type at pH 7.0.

Potential of Mean Force (PMF) Calculation. For umbrella sampling, harmonic potentials with force constant 4000 kJ/mol nm² were implemented for each of 23 windows positioned in 0.03 nm increments from 0.44 to 1.1 nm of the distance between the C_{α} atoms of P165 and Q168. The initial configurations were selected from two 10 ns MD simulations which cover the states of 3_{10} -helix to β turn (Figure 3). For Figure 6, harmonic potentials with force constant 4000 kJ/mol nm² were implemented for each of 53 windows, positioned in 0.03 nm increments from 0.44 to 2 ns of the C_{α} of Glu221 and mass center of the phenol ring of Y169. Each window consists of a sampling interval of 50 ns, and the first 10 ns of each window were not used for the PMF calculation by the weighted histogram analysis method (WHAM) as implemented in Gromacs.³⁹ Evidence for the statistical significance of the umbrella sampling for the PMF profiles is shown in Supporting Information Figure S19. To calculate the free energy difference between the 3_{10} -helical turn state and the rest, the PMF is integrated along the distance between C_{α} atoms of residues P165 and

Q168. Similar free energy differences and identical rank order of mutants were obtained using two different definitions of the 3_{10} -helical turn for the integration, i.e., distance between C_{α} atoms of P165 and Q168 smaller than 0.82 nm or distance smaller than 0.7 nm. Numerically, the area of each part is calculated using composite trapezoidal rule in a module of Scipy,⁴⁰ and the free energy is the area divided by the corresponding distance.

Construction of the Network. The clustering of 734 701 or 211 424 MD snapshots (unbiased sampling) of wild type mouse PrP^C or the Y169G mutant yields 512 or 222 clusters with 10 or more snapshots, respectively. The clusters are the nodes of the network, and the transitions between them, as observed during the MD trajectories, are edges. Note that the terms node and cluster are used as synonyms in this work. Totally there are 662 814 or 210 956 edges between nodes of wild type or Y169G mutant, respectively. The networks are plotted using a spring-embedder algorithm⁴¹ as implemented in the program igrph (cneurocvsmki.kfki.hu). The overall features of the network are robust with respect to the choice of the thresholds on link and node size.

Cut-Based Free Energy Profile. The cut-based free energy profile is a projection of the free-energy surface that takes into account all pathways to the reference state and thus preserves the barriers.^{15,16} First, the snapshots saved from the PMF umbrella sampling simulations were clustered with the tree-like algorithm (*vide supra*)³⁷ and used to determine the transition matrix. Then, the mean first passage time (mfpt) to the reference state was calculated from the transition matrix, and the mfpt was employed as progress variable to sort the clusters along the profile. The values of mfpt and the cut-based free energy profiles were calculated by the program WORDOM.³⁶ The MD trajectories of the umbrella sampling along the distance between the C_{α} atoms of P165 and Q168 were employed for the cut-based profile as they show better convergence than the conventional sampling. As for the PMF calculation, the first 10 ns of each 50 ns window of the umbrella sampling was considered equilibration and thus neglected.

■ ASSOCIATED CONTENT

● Supporting Information

Time series of distances, structural overlap of conformations from MD simulation and NMR, distributions of solvent accessible surface, SAPPHERE plot for Y169G mouse prion, PMF calculations using different temporal lengths of the individual windows in umbrella sampling, and distance of R164 CZ to D178 CG in the wild type simulations. This material is available free of charge via the Internet at <http://pubs.acs.org>.

■ AUTHOR INFORMATION

Corresponding Authors

dhuang@bioc.uzh.ch
caflisch@bioc.uzh.ch

Notes

The authors declare no competing financial interest.

■ ACKNOWLEDGMENTS

We thank Nicolas Blöchliger, Min Xu, and Andreas Vitalis, for help with the SAPPHERE plot. We also thank Dimitrios Spiliotopoulos for interesting discussions. The simulations were carried out on the Schrödinger compute cluster at the University of Zurich. This work was supported financially by a grant of the Swiss National Science Foundation to A.C.

■ REFERENCES

(1) Anderson, R. M.; Donnelly, C. A.; Ferguson, N. M.; Woolhouse, M. E.; Watt, C.; Udy, H.; MaWhinney, S.; Dunstan, S.; Southwood, T.; Wilesmith, J.; Ryan, J.; Hoinville, L.; Hillerton, J.; Austin, A.; Wells, G. *Nature* **1996**, *382*, 779–788.

- (2) Prusiner, S. B. *Science* **1982**, *216*, 136–144.
- (3) Riek, R.; Hornemann, S.; Wider, G.; Billeter, M.; Glockshuber, R.; Wüthrich, K. *Nature* **1996**, *382*, 180–182.
- (4) Gossert, A. D.; Bonjour, S.; Lysek, D. A.; Fiorito, F.; Wüthrich, K. *Proc. Natl. Acad. Sci. U.S.A.* **2005**, *102*, 646–650.
- (5) Damberger, F. F.; Christen, B.; Pérez, D. R.; Hornemann, S.; Wüthrich, K. *Proc. Natl. Acad. Sci. U.S.A.* **2011**, *108*, 17308–17313.
- (6) Christen, B.; Damberger, F. F.; Pérez, D. R.; Hornemann, S.; Wüthrich, K. *Proc. Natl. Acad. Sci. U.S.A.* **2013**, *110*, 8549–8554.
- (7) Nelson, R.; Sawaya, M. R.; Balbirnie, M.; Madsen, A. Ø.; Riek, C.; Grothe, R.; Eisenberg, D. *Nature* **2005**, *435*, 773–778.
- (8) Sawaya, M. R.; Sambashivan, S.; Nelson, R.; Ivanova, M. I.; Sievers, S. A.; Apostol, M. I.; Thompson, M. J.; Balbirnie, M.; Wiltzius, J. J.; McFarlane, H. T.; Madsen, A.; Riek, C.; Eisenberg, D. *Nature* **2007**, *447*, 453–457.
- (9) Kurt, T. D.; Bett, C.; Fernández-Borges, N.; Joshi-Barr, S.; Hornemann, T.; Rüllicke, S.; Castilla, J.; Wüthrich, K.; Aguzzi, A.; Sigurdson, C. J. *J. Neurosci.* **2014**, *34*, 1022–1027.
- (10) Kurt, T. D.; Jiang, L.; Bett, C.; Eisenberg, D.; Sigurdson, C. J. *J. Biol. Chem.* **2014**, *289*, 10660–10667.
- (11) Gorfe, A. A.; Caflisch, A. *FASEB J.* **2007**, *21*, 3279–3287.
- (12) Rossetti, G.; Cong, X.; Caliendo, R.; Legname, G.; Carloni, P. *J. Mol. Biol.* **2011**, *411*, 700–712.
- (13) Meli, M.; Gasset, M.; Colombo, G. *PLoS One* **2011**, *6*, e19093.
- (14) Scouras, A. D.; Daggett, V. *Protein Eng. Des. Sel.* **2012**, *25*, 243–249.
- (15) Krivov, S.; Karplus, M. *J. Phys. Chem. B* **2006**, *110*, 12689–12698.
- (16) Krivov, S. V.; Muff, S.; Caflisch, A.; Karplus, M. *J. Phys. Chem. B* **2008**, *112*, 8701–8714.
- (17) Rao, F.; Caflisch, A. *J. Mol. Biol.* **2004**, *342*, 299–306.
- (18) Hammond, G. S. *J. Am. Chem. Soc.* **1955**, *77*, 334–338.
- (19) Blöchliger, N.; Vitalis, A.; Caflisch, A. *Comput. Phys. Commun.* **2013**, *184*, 2446–2453.
- (20) Blöchliger, N.; Vitalis, A.; Caflisch, A. *Sci. Rep.* **2014**, *4*, 6264.
- (21) Christen, B.; Hornemann, S.; Damberger, F. F.; Wüthrich, K. *J. Mol. Biol.* **2012**, *423*, 496–502.
- (22) Gsponer, J.; Haberthür, U.; Caflisch, A. *Proc. Natl. Acad. Sci. U.S.A.* **2003**, *100*, 5154–5159.
- (23) Bemporad, F.; Taddei, N.; Stefani, M.; Chiti, F. *Protein Sci.* **2006**, *15*, 862–870.
- (24) van Rheede, T.; Smolenaars, M. M.; Madsen, O.; de Jong, W. W. *Mol. Biol. Evol.* **2003**, *20*, 111–121.
- (25) Bartz, J. C.; McKenzie, D. I.; Bessen, R. A.; Marsh, R. F.; Aiken, J. M. *J. Gen. Virol.* **1994**, *75*, 2947–2953.
- (26) Baral, P. K.; Swayampakula, M.; Rout, M. K.; Kav, N. N.; Spyropoulos, L.; Aguzzi, A.; James, M. N. *Structure* **2014**, *22*, 291–303.
- (27) Goldfarb, L. G.; Petersen, R. B.; Tabaton, M.; Brown, P.; LeBlanc, A. C.; Montagna, P.; Cortelli, P.; Julien, J.; Vital, C.; Pendelbury, W. W.; Haltia, M.; Wills, P. R.; Hauw, J. J.; McKeever, P. E.; Monari, L.; Schrank, B.; Swergold, G. D.; Autilio-Gambetti, L.; Gajdusek, D. C.; Lugaresi, E.; Gambetti, P. *Science* **1992**, *258*, 806–808.
- (28) Corsaro, A.; Thellung, S.; Bucciarelli, T.; Scotti, L.; Chiovitti, K.; Villa, V.; D'Arrigo, C.; Aceto, A.; Florio, T. *Int. J. Biochem. Cell Biol.* **2011**, *43*, 372–382.
- (29) Bernstein, F. C.; Koetzle, T. F.; Williams, G. J.; M, E. F.; Brice, M. D.; Rodgers, J. R.; Kennard, O.; Shimanouchi, T.; Tasumi, M. *Arch. Biochem. Biophys.* **1978**, *185*, 584–591.
- (30) Spoel, D. V. D.; Lindahl, E.; Hess, B.; Groenhof, G.; Mark, A. E.; Berendsen, H. J. C. *J. Comput. Chem.* **2005**, *26*, 1701–1718.
- (31) Best, R. B.; Zhu, X.; Shim, J.; Lopes, P. E.; Mittal, J.; Feig, M.; MacKerell, A. D. *J. Chem. Theory Comput.* **2012**, *8*, 3257–3273.
- (32) Hess, B.; Kutzner, C.; van der Spoel, D.; Lindahl, E. *J. Chem. Theory Comput.* **2008**, *4*, 435–447.
- (33) Jorgensen, W. L.; Chandrasekhar, J.; Madura, J.; Impey, R. W.; Klein, M. L. *J. Chem. Phys.* **1983**, *79*, 926–935.

- (34) Darden, T.; York, D.; Pedersen, L. G. *J. Chem. Phys.* **1993**, *98*, 10089.
- (35) Bussi, G.; Donadio, D.; Parrinello, M. *J. Chem. Phys.* **2007**, *126*, 014101.
- (36) Seeber, M.; Cecchini, M.; Rao, F.; Settanni, G.; Caffisch, A. *Bioinformatics* **2007**, *23*, 2625.
- (37) Vitalis, A.; Caffisch, A. *J. Chem. Theory and Comput* **2012**, *8*, 1108–1120.
- (38) Vitalis, A.; Pappu, R. V. *J. Comput. Chem.* **2009**, *30*, 673–699.
- (39) Kumar, S.; Rosenberg, J. M.; Bouzida, D.; Swendsen, R. H.; Kollman, P. A. *J. Comput. Chem.* **1992**, *13*, 1011–1021.
- (40) Oliphant, T. E. *Comput. Sci. Eng.* **2007**, *9*, 10–20.
- (41) Fruchterman, T. M. J.; Reingold, E. M. *Software - Practice and Experience* **1991**, *21*, 1129–1164.
- (42) Kabsch, W.; Sander, C. *Biopolymers* **1983**, *22*, 2577–2637.